A CRS4 spallation Target for ESS

Simulations with starccm+V5.0

V. Moreau,

CRS4, Centre for Advanced Studies, Research and Development in Sardinia

July 16th 2010
Version 1.0

Abstract

In this document, we present a series of CFD simulations performed with starccm+V5 to build a sound proposal of windowless channel spallation target for ESS. The simulations increase progressively in complexity. The first simulation is a simple Mercury loop under the effect of a pulsed proton beam. The second one also includes a Hg/vacuum dynamic interface, using the VOF algorithm. The last simulations consider a LBE loop under vacuum subject to the thermal interaction with a proton beam, and is the basis for the proposal to ESS, still using the VOF algorithm. The simulation could be completed in a satisfactory way thanks to the use of a specific sharpening algorithm. This algorithm is explained and commented. The last simulations implementation is also described in details. The final results are shown. They appear very satisfying because the sharpening algorithm performs very well without giving rigidity to the free-surface and because the design elaborated seems a very promising basis for an ESS spallation target.

Contents

1 Introduction

In the framework of the international collaboration on the future European Spallation Source (ESS)**[1**], in a preliminary conceptual phase during 2010, a Target Station Concept Selection (TSCS) working group has been formed with the aim of making an evaluation of the different target concepts already developed around the world to see which ones are more suited and easily adapted to the ESS objectives. The main critical component of the Target Station is the Spallation Target. This target must dissipate about 2.8 MW from a 2 mA, 2.5 GeV spallation beam (with a conservative 56% thermal efficiency) within a relatively short space.

In the PDS-XADS[1] FP5 project **[2**], a windowless channel like target has already been dimensioned and simulated for a relatively similar proton beam: 2.4 MWth, 5 mA and 600 Mev. In the framework of this project, the spallation target was conceived by Ansaldo and developed mainly by CRS4 and ENEA **[11**]. We investigate in this report the possibility to adapt the PDS-XADS concept (adopted as is with a simple scaling for the EUROTRANS[2] (FP6 project) **[3**] for the EFIT[3] 16 MWe target) to the ESS constraints.

The simulations performed during the PDS-XADS project were very promising. However, they were made without considering directly an eventual deformation of the free surface. It should also be noted that the room available in the ESS context is much more than in the PDS-XADS one in the flow direction while it is similarly constrained in the cross-flow direction. As former 3D simulation have demonstrated our effective capacity to perform articulated and meaningful free-surface flow simulations **[5**], **[6**], we investigate in this document the possibility to adapt the knowledge gained in PDS-XADS and the new free surface capability in the ESS context.

In parallel with the ESS framework, we are also involved in the THINS (Thermal-hydraulics of Innovative Nuclear Systems) FP7 project **[9**]. This project has been built on the consideration that several aspects of CFD need to be improved with regards to applications to heavy liquid metals in the nuclear context. These considerations have been made clear during the precedent PDS-XADS and EUROTRANS European projects. Our participation in the THINS project consists in trying to operate free-surface simulations and improve their range of application in the nuclear context both gaining know-how on existing models and also improving these models or creating new (better) ones. One of our objectives is to demonstrate the efficiency of a surface sharpening strategy lacking the usual rigidifying defect of common sharpening algorithms. The application of the algorithm for a free-surface spallation target is ideally in line with the THINS objective.

The free surface simulations are performed with starccm+ version 5.02 [4]. From this version on an internal CAD part has been included, letting the former geometric modeller, stardesign, essentially obsolete. The simulations presented here are therefore entirely elaborated in the starccm+ environment.

The main challenge of the PDS-XADS design was to organize a controlled horizontal flow in a very short space. The flow had to rise up, bend to horizontal, cross horizontally the spallation region, bend downward and sink to the lower part to be cooled down by an Heat eXchanger (HX). All this had to be performed in a cylinder of about half metre diameter. The pumping system had also to be located in this cylinder, with a relatively low pressure head, so the mass flow rate and the pressure drop in the loop were of great concern.

From a preliminary analysis of the ESS requirements, it looked like the stream-wise direction could be arbitrarily extended. With much more space to bend the flow to horizontal, one could operate in a smoother way and reduce quite a lot the pressure losses. Moreover, the pumping system could be located remotely without any power limitation due to volumetric constraints. The mass flow rate was therefore thought to be arbitrarily extendable. A very large mass flow rate, in comparison with the reference one about 220 kg/s, leads to a minimized temperature range and in consequence to a very low thermal stress. However, increasing the flow at constant geometry leads to the destabilisation of the free surface which become more and more agitated. Therefore, an optimum could be reached by maximising the mass flow rate for a minimum acceptable free-surface unsteadiness.

[1] Preliminary Design Study of an eXperimental Accelerator Driven System
[2] EUROpean research programme for the TRANSmutation of high level nuclear waste in an accelerator driven system
[3] European Facility for Industrial Transmutation

In the following, we present the main simulations performed to arrive to a consistent update of the windowless channel spallation target for the ESS purpose. These simulations, starting from an extremely simple dimensioning check, progressively took into account the information released during the 2010 TSCS working group meeting, and also took profit of bilateral working meetings with the TSCS head. The time evolution of the channel target is reproduced hereafter.

This paper is organized as follows. First, we deal with the trouble shootings of numerical implementation nature we have been faced with, and the way we have bypassed them. These trouble shouting are extremely important for the CFD engineers because they usually delay the results by a factor of 2 or 3. For complex simulations such as the one presented here, they can simply impedes the production of any meaningful result. As we would like our simulations to be easily repeatable, with give the trouble shouting this place of choice.

Second, we deal with a very simple Mercury loop. This loop served mainly as support to the discussion and for preliminary numerical settings and controls. The loop was run without free-surface but with a sufficient time accuracy to capture the individual beam pulses.

From the considerations on this Hg loop, we then (third) build a quite more elaborated one, comprehensive of a free-surface simulations. One gets there at the heart of the free-surface issues where steady states are unlikely but surface waves are not.

At the time the second Hg loop was ready, it turned out that Hg was highly problematic for reasons mainly related to dismantling issues. Therefore, Hg would have to be substituted by LBE or Lead. We shortly discuss the pro and con of LBE versus Hg. Then we gather all the physical and numerical information to build what will be the layout of a LBE windowless spallation target channel for ESS. We give a quite detailed description of the geometry, the mesh and overall of the numerical implementation. More specifically, we explain in detail how we could manage to perform a free-surface flow in a loop with thermal coupling. This has been made possible only thanks to a simple but essential change in the VOF algorithm. The change is abundantly explained and discussed. The results of five simulations, with two different flow rates and three different beam shapes are then given.

2 Trouble shootings

It has been found out that the second order temporal discretization gave a much better (cleaner) result for the first Hg loop. So, we tried to keep this discretization for the LBE loop. Unfortunately, the temperature in presence of both 2^{nd} order and VOF was systematically and un-physically diverging in time, the heavy fluid becoming hotter and the light fluid becoming much cooler. This obviously before any beam source term. Added under-relaxation of temperature and/or VOF gave no amelioration. Idem with fixed physical properties, smaller time steps. Only reverting to first order time discretization led to a correct temperature behaviour.

Also, combining an heavy fluid variable density (with only temperature dependence) with VOF resulted in a simulation crash. This is expected to be a bug solved in a further release. Anyway, it has been possible to investigate directly the buoyancy eventual effects only up to the Boussinesq approximation through the introduction of an additional body force.

It has been impossible to completely stabilize the light velocity phase just over a stagnant heavy phase. When and were the heavy phase free-surface is stagnant, the light phase velocity presents a patchwork aspect with velocities varying locally in space with values up to about 1 m/s in any direction. This effect disappears as soon as and everywhere the free-surface flow is moving. As it does not seem to have any consequence on the heavy flow behaviour, this effect has been ignored.

The final simulation with LBE (fast case, fitted beam) could be completed only up to 80% (4s over 5 s) seemingly because of a problem with the java interface capturing automatically the scenes to make transient animations. As the results were definitively in favour of the slow case configuration, the incomplete simulation has been let in its current state.

3 First Mercury loop

A first simulation with Mercury based on these considerations has been performed. The simulation was 3D transient with a sufficient time definition (1 ms) to represent crudely the 20 Hz pulsed beam with 2 ms long pulses. The simulation, however, was performed with a fixed free-surface with no-slip boundary condition. It could be used as a preliminary simulation either for a free-surface target or for a thin window target, for which the temperature could be loosely estimated. The Hg loop was initially built for LBE which has a lower density so that the beam penetration length is greater. Only the (spatially uniform) heat release region was shortened to 60 cm, while the channel upper part is 1 m high. The pulsed heat release instantaneous intensity was 25 GW/m3 for a 4% load, giving a mean 1 GW/m3.

The mass flow rate, about 93 l/s in the simulated part (total would be 186 l/s) was dimensioned so as to have a velocity about 1.6 m/s in the spallation region, as shown in Figure 4. In such a way, the successive beam pulses almost perfectly heat juxtaposed fluid volumes. In Figure 3, on can see in the spallation region the effect of only 1ms pulse while the flow heated by the preceding 2ms pulse is just shifted to the right. The objective of the channel restriction close to the spallation region is three-fold. First, this part of the channel must be the thinner possible so that the neutron moderators can be put the closer possible. Second, the restriction makes the flow quite uniform in the spallation region. Third, the pressure gets its minimum value around the beam footprint, so that an eventual spallation window would be subject to a very low static pressure load.

An animation movie of the temperature field around the spallation region during the last 0.5s of simulation has been produced and can be released on demand.

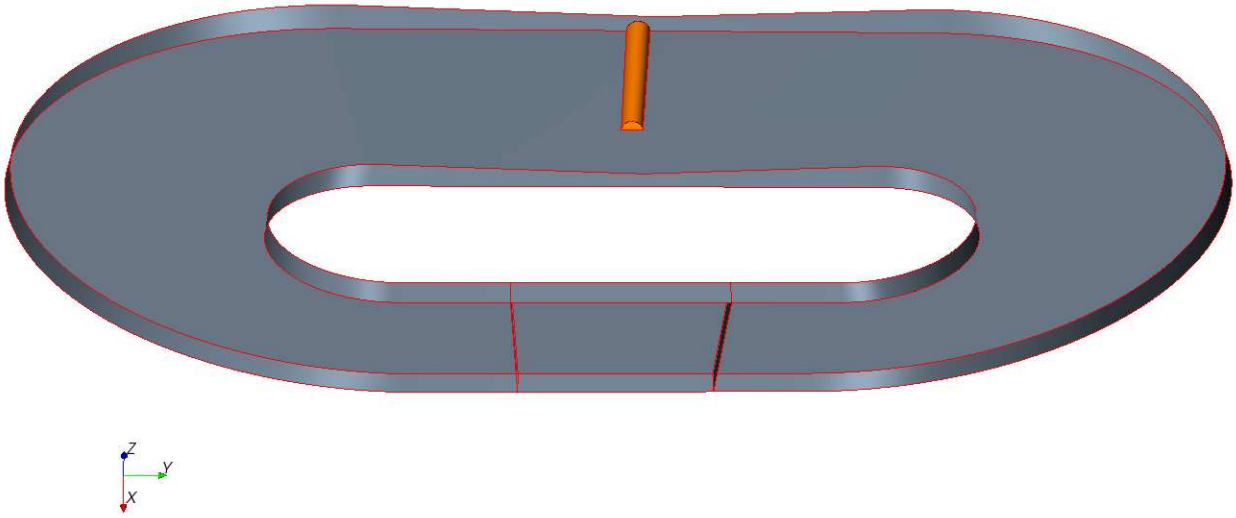

Figure 1: Geometry of the first Hg loop. Total height is 3 m. Width is 5 m. Depth is 10 cm reducing to 6 cm close to the spallation region (for the half domain simulated). The spallation is a cylinder of radius 4 cm and 60 cm high, in yellow on the figure.

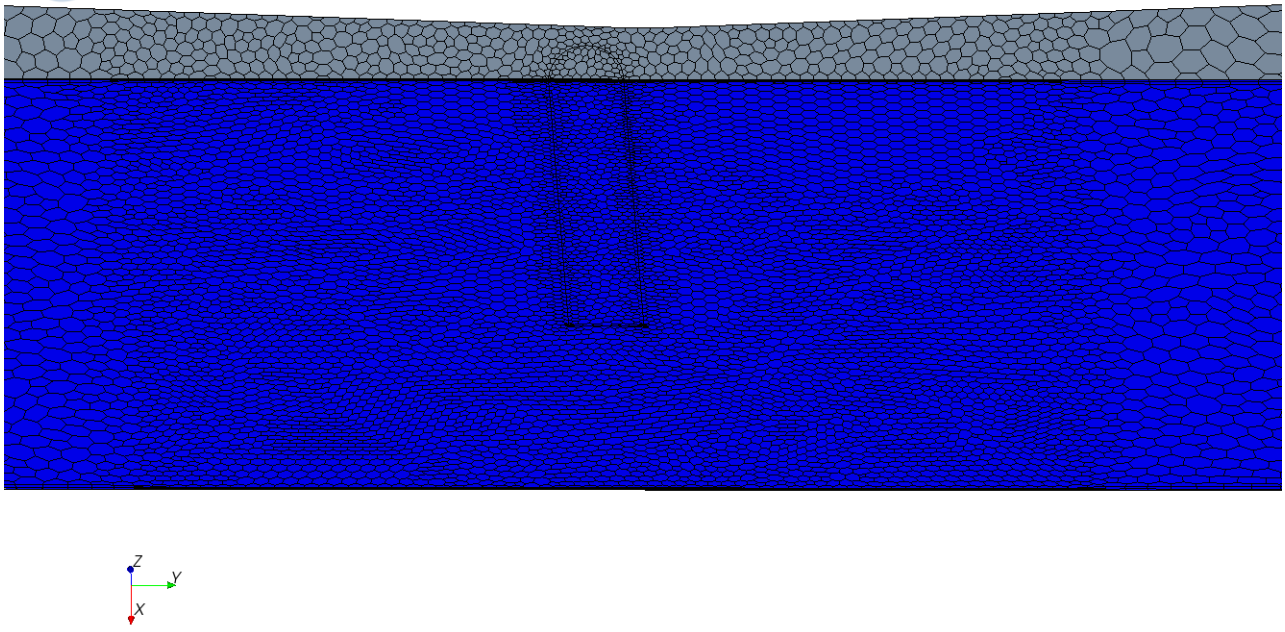

Figure 2: First Hg loop. Surface mesh detail close the spallation region.

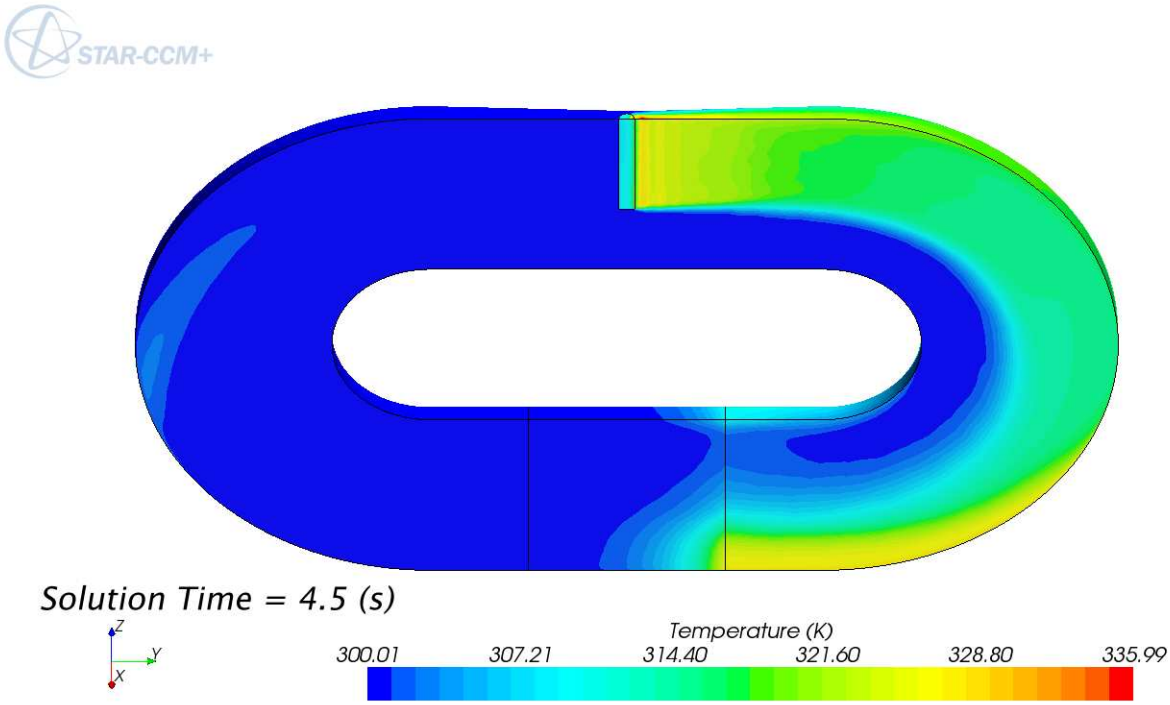

Figure 3: First Hg loop. Temperature field after 4.5 s of pulsed transient.

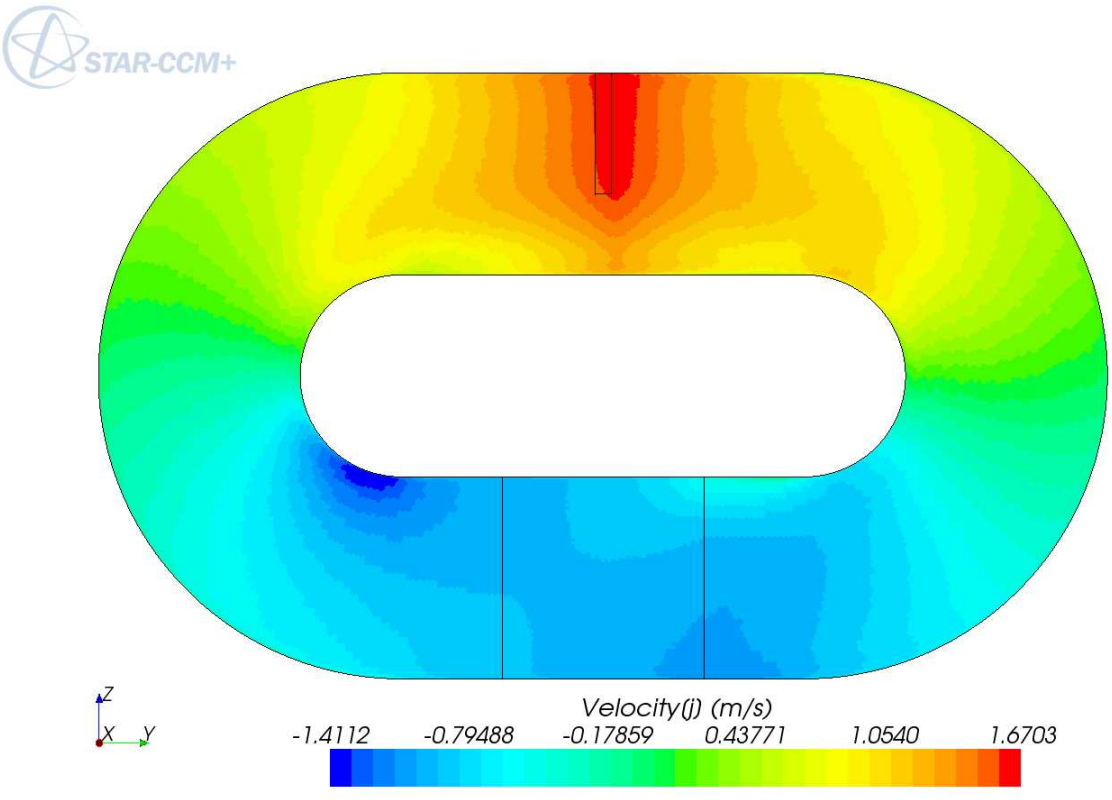

Figure 4: First Hg loop. Horizontal velocity field.

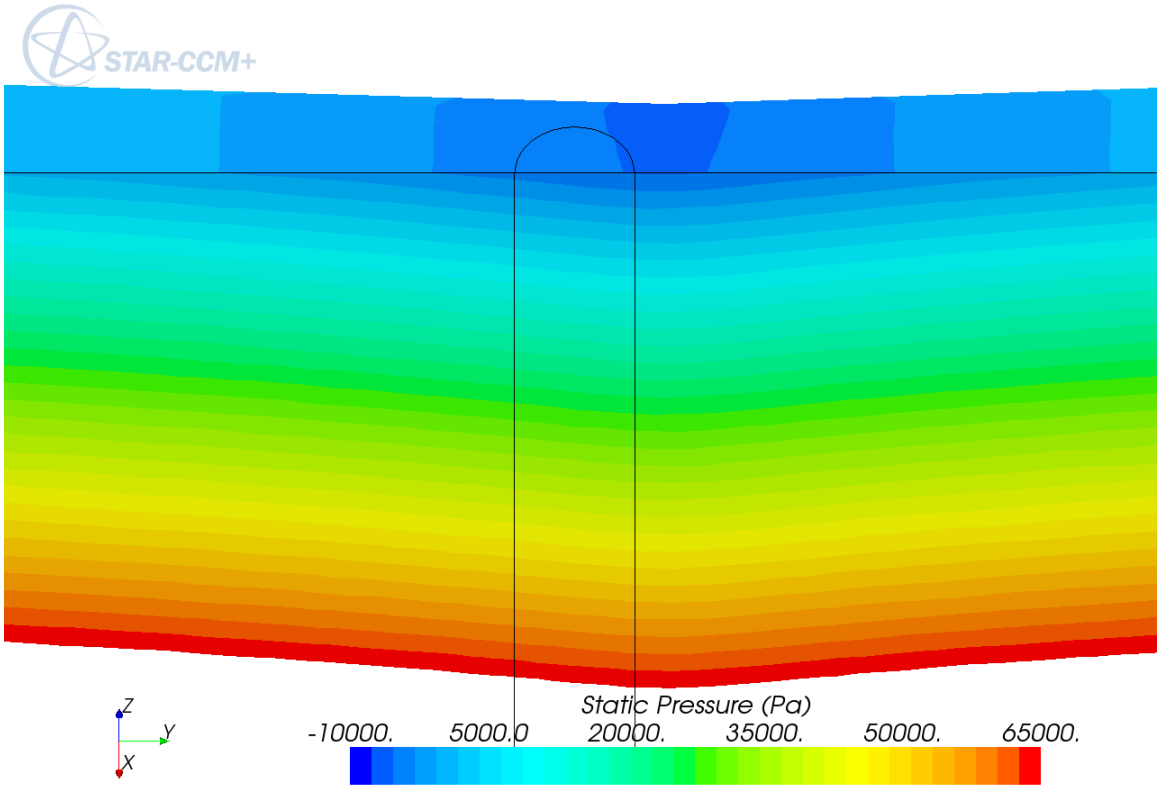

Figure 5: First Hg loop. Static pressure close to the spallation region.

4 Second Hg loop

The first Hg loop was presented to the ESS target station team in a bilateral meeting in April 2010, after a foreseen meeting in Juelich had been cancelled due to the volcano eruption in Island…

From the discussion, emerged that for mercury the evaporation issue is much more stringent than for LBE even at ambient temperature. So, in any case, the would be free surface span should be the smallest possible. Moreover, the mercury was believed to create large problems at dismantling stage, and therefore the total Hg inventory would have to be kept under control. There was also a strong reluctance to consider flow rates much higher than for other loop designs. While the free surface target is virtually without friction losses in confront with the reference target design, the friction losses in the rest of the loop, mainly the heat exchanger, was also relevant and the advantage of small target pressure losses is not so huge as to allow much more mass flow rate for similar pumping systems.

Some effort had to be put on reducing the Hg inventory and mass flow rate.

Last but no least, we had to demonstrate our technical operability in simulating coupled free-surface/ thermal flows.

A second Hg loop has been (numerically) built. It is shown in Figure 6, while the Hg volume fraction (and therefore the free-surface position) can be appreciated in Figure 7 at the end of the first simulation. In the geometry, the left “tower” was there to serve as an Hg buffer. Its free surface must be separated from the central tower one so that a slight free surface level control could be operated by controlling the pressure (always small) in this region. The central tower is the passage for the beam line. The right tower was supposed to be used for degassing, with the gas in the

central tower ideally captured by suction by the Hg flow and the upper wall. The upper wall between the left and central towers is aimed both at separating the free surface region and at creating a natural smooth flow detachment in the central region. The upper wall between the central and the left tower was expected to impedes some backward flow to bounce back to the spallation region.

The simulation has been run in several steps. First, the would be initial conditions are established. This is done setting the initial conditions, mainly zero velocity, and running the simulation for a few very small time steps with a relatively large number of inner-iterations (up to 40). This is to allow a correct pressure profile to establish without giving time to the flow to be convected by the first time-steps velocity field. After that, the driving force is turned on an the flow slowly develops. The driving force induces a movement and a deformation of the free surface. Waves are created on the free-surface, living their own life and hopefully slowly disappearing in time. Very soon, the impression on the three-towers simulation is that the flow height was excessive. So, we had to reduce the heavy liquid inventory. This was done by setting a distributed VOF sink of the heavy phase, coupled with the corresponding Enthalpy sink. The heavy fluid sink lowers the free surface but also participate to the wave strengthening. As the transient simulation is quite slow to proceed (one or two second by day), we did not wait that the waves completely disappear, if ever, and started the proton beam thermal interaction.

The simulation presented below starts for an apparently relatively stable flow configuration with a controlled total heavy fluid inventory. We do not know whether waiting longer we would have had a more stable flow or whether the free-surface instability is intrinsic of the geometry and the operating conditions.

A three second transient simulation with a coupled beam thermal interaction has been performed. Some animations of the transient simulation have been registered and can be given on demand. The final volume flow rate in the simulated domain is 62 l/s. The Hg volume fraction at the end of the simulation is presented on Figure 7. The trace of the beam thermal interaction on the symmetry plane is shown in Figure 8. The beam is pulsed. Each pulse last 2ms and the pulse frequency is 20 Hz. The instantaneous heat power deposited in the computational domain is 39 MW for a mean power of 1.56 MW. The horizontal velocity is shown on Figure 10. It turns out that the right upper wall completely fails to impedes a backward wave to travel up to the spallation region. This is still clear from Figure 9 where one can see a hot volume created during the overheating caused by the backward wave. Even if the flow seems to recover from this event by pushing away the hot volume, one can fear that other similar events may occur.

Another simulation, not illustrated here, with half the flow rate (31.4 l/s) also showed an excessive backward bouncing wave.

While with this simulation we could demonstrate the technical feasibility of such simulation, and also check some feature like the total heavy fluid inventory control and a good (sharp) representation of the free surface which is almost never wider that 2 cells, the results where not satisfying and a free-surface spallation target cannot be proposed on this geometric basis.

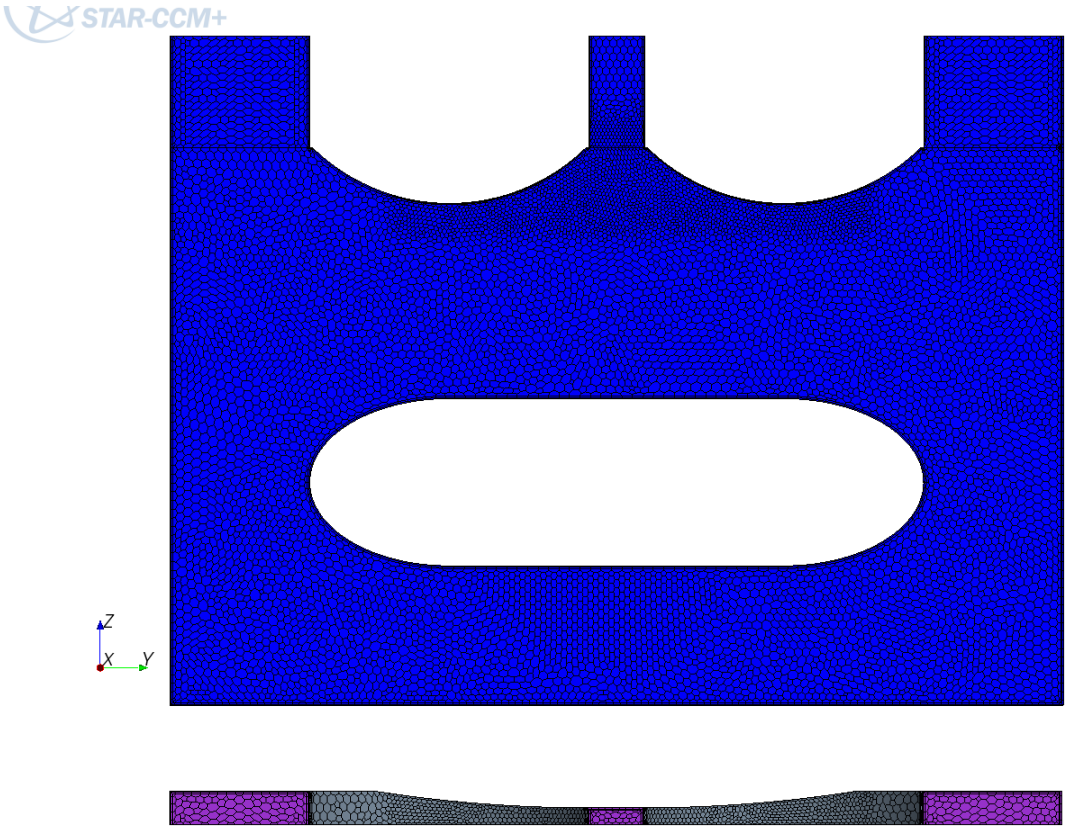

Figure 6: Second Hg loop. Geometry and mesh density. Total height is 2 + 0.4 m, width is 3.2 m. Depth (half) is 12 cm reducing to 6 cm in the central part. Up: view of the symmetry plane. Down: top view.

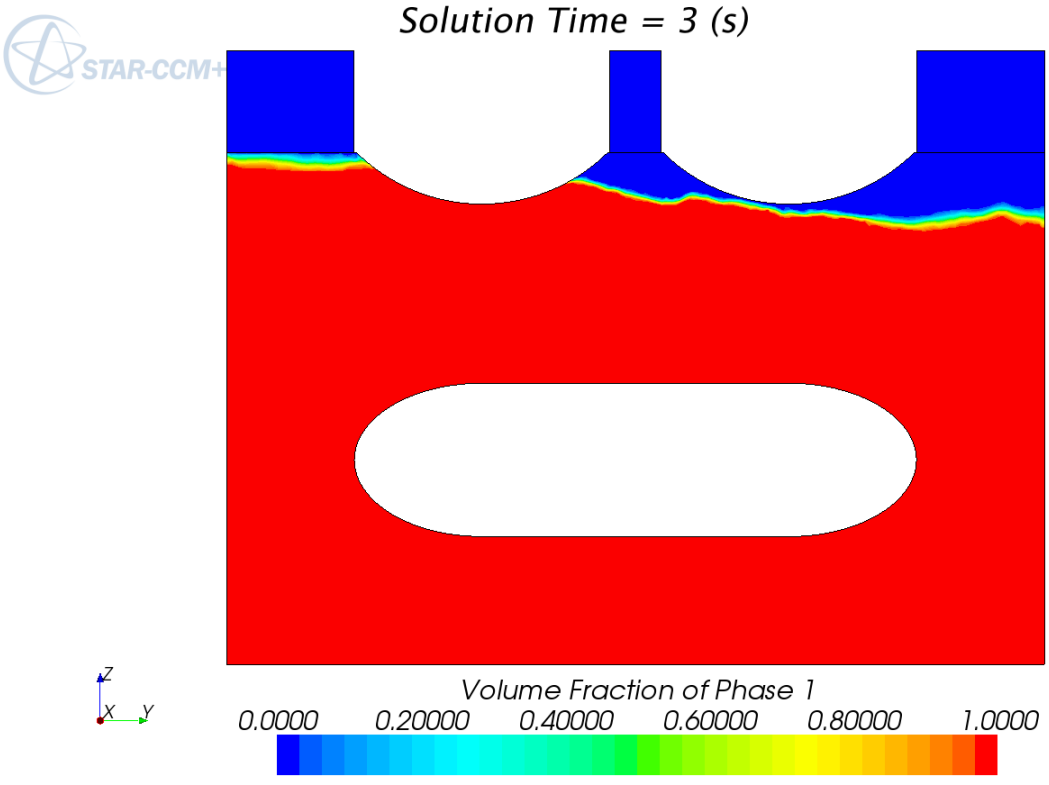

Figure 7: Second Hg loop. Hg volume fraction after 3s of pulsed beam.

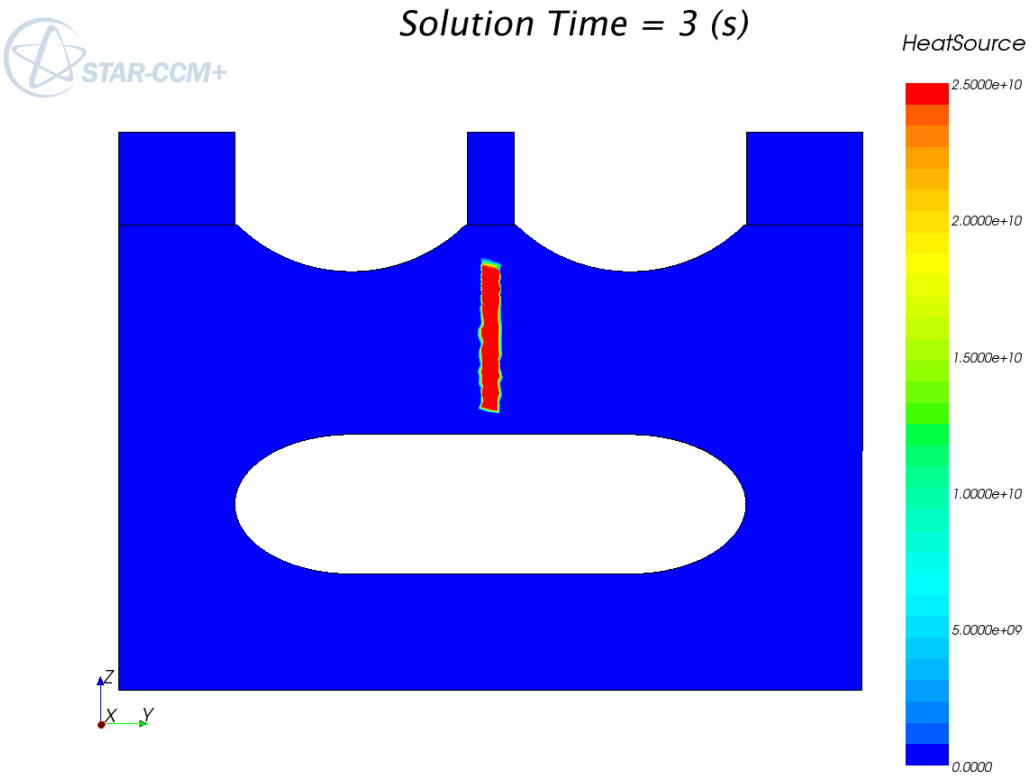

Figure 8: Second Hg loop. Instantaneous heat release deposition at 3s on the symmetry plane.

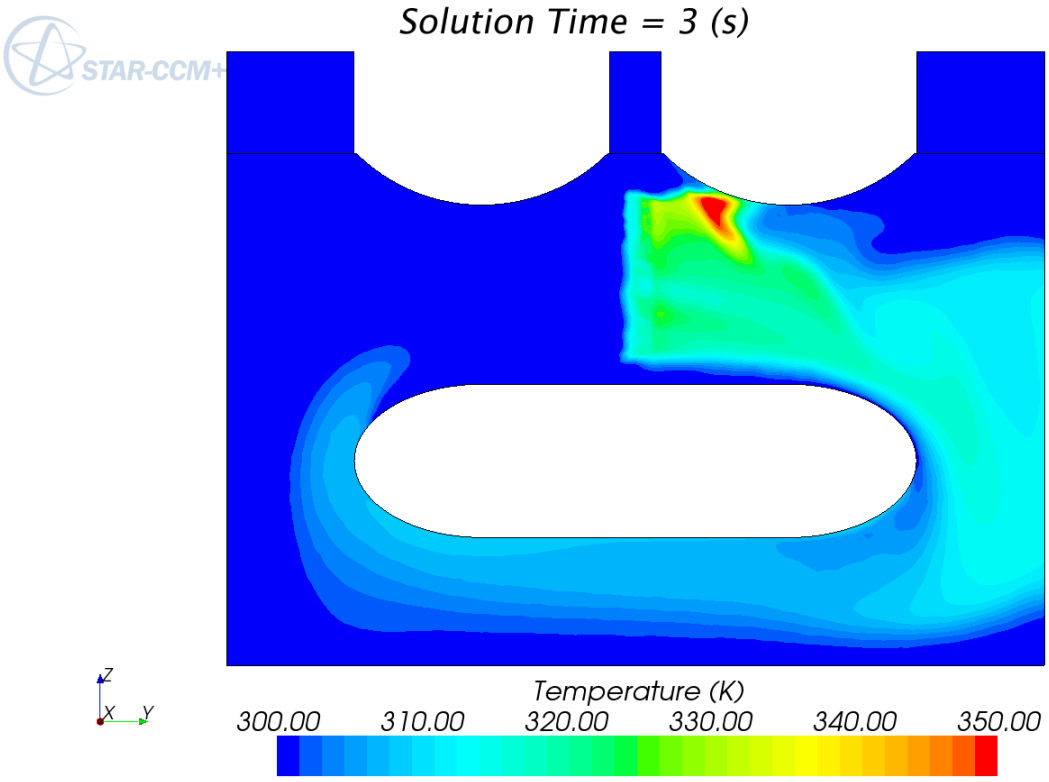

Figure 9: Second Hg loop. Temperature on the symmetry plane after 3s of pulsed beam.

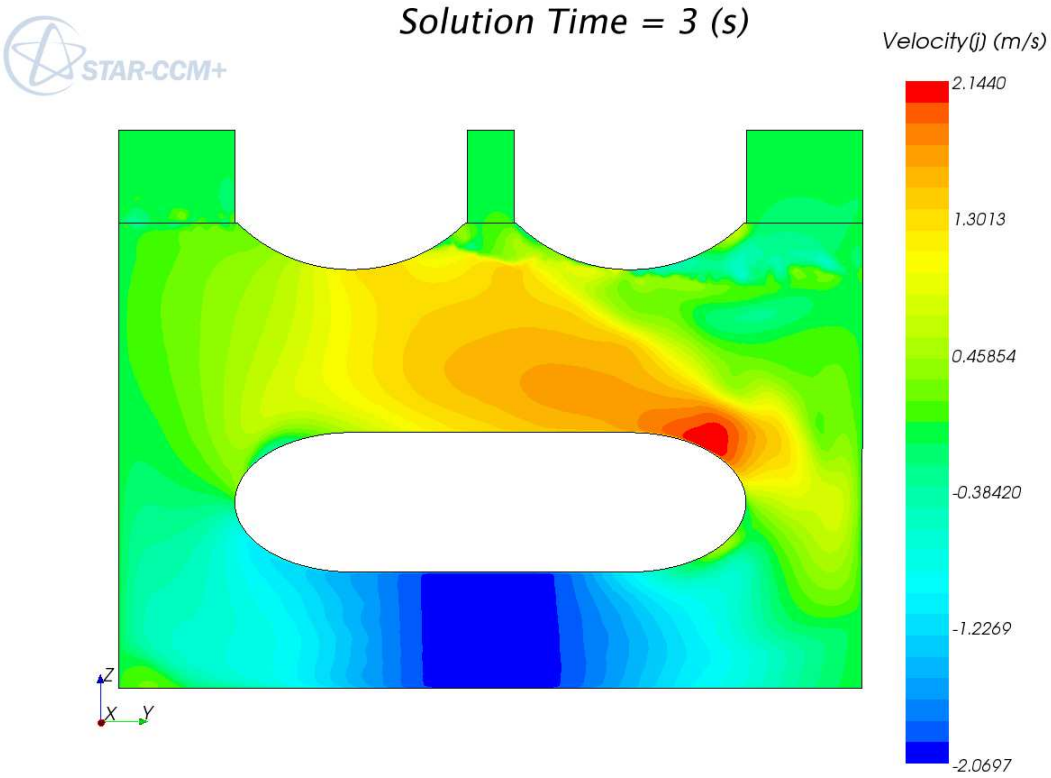

Figure 10: Second Hg loop. Horizontal velocity on the symmetry plane at 3s.

5 LBE loop

An ESS spallation target meeting occurred during the former simulations run (TSCS meeting in Juelich 15-16 June 2010). During the meeting, it has been made clear with a presentation made by P. Zimmermann [4] that the use of Hg as spallation material would be faced with huge accreditation issues related to safety, and mainly to decommissioning. Therefore, an Hg spallation target proposal was almost surely doomed to failure.
A few days after, we had a bi-lateral meeting with the ESSS target team. During this meeting, the Mercury issue was confirmed and we tried to put the basis on reasonable constraints and objectives to switch to an LBE loop.

5.1 LBE vs Hg

The main advantages of Mercury were two. It can be operated at room temperature and it has a large specific weight. In all the discussions performed with the ESS team, the first advantage was considered negligible. Worse, some people retained that is would be better to operate at a much higher temperature as it would be beneficial for the self-healing properties of the strongly irradiated materials. The fact that the moderators had to be put the closer possible to the target and that they must be operated at 4K was not considered an issue. So, reducing the temperature gap between the moderators and the target is not considered an added value at this stage of the project.
With regards to these two properties, LBE is only slightly lighter than Hg, its density being about 25% less (still about 10.5…) and its melting temperature is quite low: 398K (125 C). However LBE has other extremely beneficial features. Its boiling temperature is 1943K while the Hg one is

[4] P. Zimmermann, H.-F. Beer, Paul Scherrer Institute. Manadgement of Radioactive Hg, Methods, Problems, Costs

only 630K. The LBE vapour pressure is extremely low, below 0.014 Pa up to 550 C, a value practically never reached by Hg (except a few degrees close to the melting point at -39C).
Taking into account that large flow rates are not welcome, one must cope with non negligible temperature variations (at least 100 K, but eventually much more) and to be compatible with an almost perfect vacuum (0.01 Pa), only LBE (that is, not Hg) allows to potentially build a free surface spallation target with a limited mass flow rate. From a practical point of view, if the LBE free-surface temperature is kept below 550 C, then there is no need to restrict its span, because the evaporation is no more an issue.
As a spallation target material, LBE has one inconvenient. It produces a large amount of Polonium. Polonium is only considered a highly toxic venom, so either one as to find a useful application for it[5], or one has to deal with its treatment and neutralization.
While not giving any solution to this issue, one should note that the CDT European project **[7**] foresees the realization of a Fast Spectrum transmutation Facility (FASTEF) in Mol (Belgium) with LBE serving both as spallation target and core primary coolant. The foreseen LBE inventory is about 4,000 Tons **[10**], at least two orders more than the one foreseen for ESS, and all this LBE will be highly contaminated with Polonium. Therefore, solutions for the Polonium issue will have to be implemented in the CDT framework and these solutions have high probability to be satisfactorily applicable to the ESS Polonium.
Another way to get rid of the Polonium issue is to get rid of the Bismuth in the LBE, that is, use molten lead as coolant. The only real difference in operating with Lead or LBE is the operating temperature which should sufficiently over the Lead melting point at 600 K (200 K higher than LBE). From the CFD point of view, all the simulations performed with LBE can be straightforwardly reinterpreted for liquid Lead with good accuracy.

5.2 Beam line orientation

Apart from changing the spallation target material, we also considered the beam orientation issue. With the increasing beam energy foreseen (2.5 GeV), bending magnets become more and more large, more and more heavy. Up to the point that putting a magnet exactly over the spallation source risks to overweight the structure. While magnets are present in all comprehensive beam line designs, magnets that bend the beam 90 degrees will be avoided. By the way, a down-coming beam inclined 30 to 60 degrees with the vertical is perfectly foreseeable, or even preferred. Therefore we agreed to consider a beam inclined 45 degrees to the vertical.

5.3 LBE loop geometry

A complete loop has been built (up to the geometric symmetry). A bottom tubular region with diameter 30 cm has been dedicated to the resetting of the temperature and furnished with a distributed momentum source simulating a generic pumping device. The bottom horizontal pipe is bent vertically to enter a buffer region with a relatively stagnant top free-surface. This buffer region connects smoothly to a 8 cm wide (4 cm in the simulation domain) and 60 cm high straight channel through a connector with a reducing width. The straight channel is dedicated to the spallation region. The beam interact from the top with the flow in this channel after a while to let the channel recover from the contraction. After the spallation region, the flow enters laterally into a vertical cylinder 30 cm large, curving back at the bottom to complete and close the loop. At the free-surface level in this last cylinder, we introduce a flow diverter whose shape is inspired by a ship prow,

[5] In this context, the elimination of political opponents should not be considered a useful application for Polonium.

cutting the incoming flow such that no backward waves occur. The complete geometry is illustrated in Figure 11 together with the mesh which is refined to better capture both the free surface shape and the beam energy deposition.

Making profit of the vertical planar symmetry, the overall simulation domain is enclosed in a box whose dimension are (X,Y,Z)=(1.9, 0.15, 1.25)m^3. The mesh is composed of about 800,000 cells. It is composed of both polyhedral cells in the bulk and two boundary prismatic cell layers. The mesh cell base dimension is 12 mm with two level of volumetric control refinements at 6 and 3mm.

5.4 LBE physical properties

The physical properties of LBE are taken from the LBE handbook**[8**] and are reported in Table 1. Note that the extremely low vapour pressure at 300 C can be better understood observing that at this temperature, Lead is solid (while Bi melts at 271.5 C). Specific Heat, viscosity and thermal conductivity are simulated as in the table. In starccm+ version 5.02, it has not been possible to use together the Volume Of Fluid (VOF) feature and a temperature dependant density, trials leading to an apparently software crash (not to divergence of the flow). Buoyancy may lead to devastating effects, manly at very low flow rate, leading to thermal lock phenomena. It is therefore necessary to take it into account. This has been done by reverting to the Boussinesq approximation for buoyant flow, which is very commonly used for incompressible flows because one can still profit of the divergence free property of the velocity field and keep the general features of buoyant flows.

The approximation consists in keeping the density constant to a reference temperature density T_0 (here 573 K) and to introduce a body force in the momentum equation proportional to gravity and would be density variation to the reference one. Reported in terms of the temperature, it gives:

$f=a\,(T-T_0)\,g$, where a=-1.3236 is the coefficient in the density formula and g is the gravity vector.

In the VOF context, the Boussinesq force f is multiplied by the LBE volume fraction before being applied to the overall momentum equation.

5.5 Source terms

The pseudo-heat exchanger (HX) is roughly simulated by an Enthalpy sink in the temperature equation. It is applied on 1m length of the bottom tube. It has the very simple form:

$S=\rho\, C_p(T_0-T)/\tau$, where T_0 is the objective temperature for the cold flow (still 573 K) and τ a characteristic time such that the flow needs several times τ to travel across the HX. This form is believed to be the simplest not aggressive one.

The driving force is done in the same way. It is a force applied to the momentum equation and localized in the pseudo-HX (for simplicity and compactness, not for realism). It is horizontally oriented and has the following form:

$f_x=b\ \rho\,(v_0-v_x)$, where v_0 is the objective velocity in the pipe, v_x its current velocity and b a strength parameter (dimension s^{-1}) such that for b large enough in confront with the loop hydraulic resistance, the asymptotic flow velocity in the pipe tends (by inferior value) to v_0. A final value of b=5 has been used, but the value is lower at the beginning of the simulation (starting from stagnant flow) to avoid the formation of catastrophic surface waves.

Two simulation series have been run (almost) in parallel. One with v_0=0.5 m/s for a so called slow flow case and the other with v_0=0.7 m/s called fast flow. The slow flow settles about 14 (28) l/s and the fast flow about 19.5 (39) l/s. Number in parenthesis refer to the entire physical domain and not only to the half simulated part.

The VOF simulations tend to exhibit a very slow mass (VOF) loss. This is specially true in presence of highly disturbed surface flows. The small discrepancy in the heavy fluid volume conservation is usually not noticed and can be attributed to boundary conditions. For a closed loop, the mass loss (or gain) in time is more easily noticed because it can accumulate in time. In former simulations, we could observe that part of the mass variation was reversible. That is, a pseudo-periodic flow with a large change in the flow topology would give a similar oscillation of the measured mass. It is therefore possible that part of the mass variation is only due to the starccm+ internal measurement method. Anyway, there still was a mass variation from one cycle to the other, slowly accumulating in time. The reason may be found in the level of convergence of the pressure equation and may be due to an excessive local courant number in part of the free-surface location. Whatever the reason, we want to work with a preserved LBE mass and a source term has been added to the VOF equation, heavy fluid part, in the usual form:

$S=(m_0-m)/m_{HX}/\tau$, where m_0 is the (measured) initial mass of LBE, m is the currently measured mass of LBE, m_{HX} is the HX mass when filled with LBE because the source is localized only there and τ the usual characteristic time of return to equilibrium. We have taken τ=0.2s. Once again, we believe this form to be the simplest not aggressive one. Truly, this form do not stress the algorithm convergence only if is applied from the beginning of the simulation or with reference to the LBE inventory at the time the source is started.

5.6 Temporal setting

The time step as been set after a while to 4 ms. The inner iterations have been reduced from the initial default 20 to 8. The time step is chosen so as to have the local Courant number almost always not too much over 1, at least close to the free surface in the spallation region. With the smallest mesh characteristic size of 3 mm and a velocity only marginally over 1 m/s, the objective is reached.

We should stress the fact that the usual recommendation for sharp VOF flows is to keep the maximum Courant Number below 0.3. In our case, as we really need a sharp interface, the 3mm size is not “negotiable” in the spallation region. With a 4 ms time step, 8 iteration by time step we simulate about 2s of flow by day. The flow needs more than 10 s to develop and reasonably quiet down so that we can start to light the beam. Beam interaction should last at least 5s (better 10s) to get a sufficient feeling on the surface asymptotic temperature and behaviour. So, we are faced with simulations during weeks. Reverting to the recommended 1ms time steps, weeks become months. Keeping the default 20 iteration by time step would make it even worse.

This last consideration is better understood taking into account that real transient simulations, that is, simulation not converging necessarily to a steady state, almost never meet the internal criteria for inner iteration convergence, specially, as it is always our case, when we make use of several source terms.

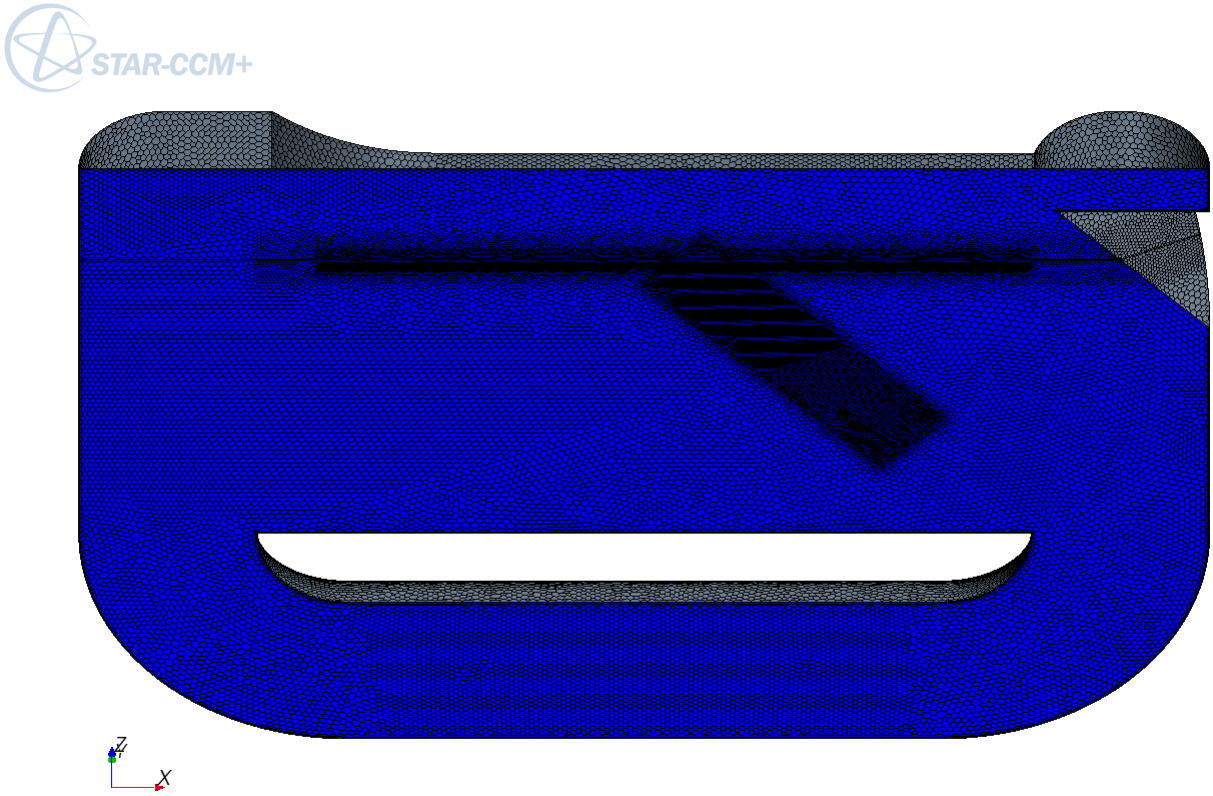

Figure 11: LBE loop simulation domain with surface mesh. The flow is supposed to be clockwise.

Property	SI unit	Correlation	Temperature range (K)	Value at 573 K
Saturated Vapour pressure	Pa	P_s=11.1E9*exp(-22552/T)	508-1943	9.0E-8
Density	$Kg.m^{-3}$	ρ=11096 – 1.3236T	403-1300	10338
Isobaric specific Heat	$J\ kg^{-1}\ K^{-1}$	C_p=159-2.72E-2 T + 7.12E-6 T^2	430-605	146
Dynamic viscosity	Pa s	η=4.94E-4 exp(754.1/T)	400-1100	1.84E-3
Thermal conductivity	$W\ m^{-1}\ K^{-1}$	λ=3.61+1.517E-2 T - 1.741 E-6 T^2	403-1100	11.7

Table 1: Recommended correlations for main thermo-physical properties of molten LBE (p~0.1MPa)

5.7 VOF improvement

We have seen in the temporal setting that our simulation is performed with much higher Courant number than recommended. However, we maintain a very sharp free-surface, and easily re-contract the surface when it has been smeared due for example to the brake up of a wave. This has been done without reverting to the starccm+ sharpening algorithm because it is presented as giving rigidity to the surface and is sensitive to the cell orientation, if ever. In the animations showing the temporal evolution of the free surface, the free-surface do not seem to suffer from an increased rigidity. And no specific effect is visible when the free-surface crosses the only horizontal cell layer interface. This a purely subjective but comforting impression. What is also highly appreciated is that no light flow is driven into the down-comer part.

In a normal VOF flow, some light phase should be transported by the heavy phase all around the loop. Because, with reversal flows, bubbles are forming and small bubbles are always transported by the flow.

We are not simulating normal VOF flows, such as liquid water/gaseous air at 1 Bar pressure. We simulate a liquid flow under deep vacuum. And vacuum cannot form bubbles, at least for long. If it would, the bubble would instantaneously shrink to almost zero size as soon as the pressure becomes a few Pascal, that is a few tens of micron below a stagnant surface.

Our algorithm, while extremely simple in its implementation, is based fundamentally on this former observation.

For fluid vacuum VOF flows, whatever treatment done on the light phase should be considered as a treatment of the error. For example, the light flow density is not set by physical consideration but simply imposed by the fact that the VOF algorithm become unstable or at least extremely difficult and costly to stabilize with the increase of the density ratio. Normally, the VOF algorithms presented in literature never demonstrate to be operational at density ratio greater than 1000, so as to catch the usual water/air ratio. And it is already extremely challenging to reach stability at this value. The starccm+ VOF algorithm is quite stable at this ratio and perfectly unstable (until otherwise demonstrated…) at a ratio of 10,000 which would be the ratio for LBE/Air at under atmospheric pressure.

In practice, we are obliged to limit this ratio to 1000, so we are forced to set the “vacuum” density to about 10 kg/m^3. This is to reinforce the argument that the light phase treatment is only a treatment of an error (because the light phase is “only” error). This can be considered a bug, but may be transformed in a feature. In effect, any action (that is a modification of the driving equations) performed on the light phase treatment must only be considered through the effect that it induces on the heavy phase. So, what is good for the heavy phase is good.

As normal starccm+ users, we can act on the VOF algorithm basically only through the implementation of a dedicated source term. That will be (and is) done.

What we want to do is apparently twofold: (i) avoid “bubble” entrainment and (ii) avoid free surface smearing.

These two points are in fact only one, because “bubble” entrainment is a kind of surface smearing. Surface smearing can appear through a small volume fraction of the light phase in the heavy phase bulk, through a small volume fraction of the heavy phase in the light phase bulk, or in any intermediary more symmetrical situation.

So, we want to keep the surface sharp. Do we? Not always. There are specific situations, usually strongly localised both in space and in time in which we need to have a little smearing of the surface. The typical such situation is when a local change of topology should occur, when the

surface becomes for a short moment non-manifold. In simpler words, it occurs in situations such as the coalescence of a droplet onto the main surface or the ejection of a droplet. These are the situations for which it is neither wanted nor easy to keep the interface sharp. But when this occurs, it should not last for long and the surface should sharpen again.

Reformulating our objectives, we can say that the free-surface should not smear without serious reason, and a smeared surface should naturally sharpen back when the reason is no more. That is, we have slightly relaxed the objective of not smearing, and thus recognized the legitimacy or at least the possible occurrence of smearing. This is from on side. From the other side, we must be able to actively correct the occasional deviant behaviours. This pseudo-philosophical reformulation is not new, but is not very old either. A correspondence in the nuclear field is the passage from impeding any accident to occur to yes impede them to occur but still control the situation if (and inevitably when) they occur. In politics, it could be: “not only have peace, but also make peace”.

Now back to our VOF algorithm. Only one trivial observation remain to be made explicit, that is that problems (smearing) occur only when both phases are present. And as one of these phases is an error (the light one), one cures the problems by removing the error, that is the light phase, when the heavy phase is also present. Removing must be performed fast enough to control the propagation of error, but not too fast to let the short time licit events perform their duty.

The contemporaneous presence of both phases can be represented in the simplest way by the product of the volume fractions. So, our VOF sharpening algorithm reduces to a simple sink term in the light phase equation proportional to the product of the volumetric fractions. The coefficient of proportionality controls the speed of the process:

$S=-c(1-c)/\tau$, where c is the heavy phase volume fraction and τ the usual characteristic time.

For a thermal VOF flow, the Enthalpy of the light flow taken out must be withdrawn in the temperature equation. The corresponding Enthalpy sink term is:

$S_h= \rho C_p S$, where ρ and C_p refer to the light phase.

Some discussion can be made on the value of the characteristic time. While in exact arithmetic, this source term is identically zero for a discrete interface, in practice, the minimum free-surface width in a non structured mesh is of the order of the cell size δ. For such a minimum size, the light flow induced by the source term should not create any noticeable effect on the heavy flow structure. Moreover, it should not jeopardize the interpretation of velocity plots. So, a sound limit could be to induce a light flow velocity at least one order less than the typical heavy fluid velocity v, that is:

$\delta/\tau < 0.1*v$.

As c(1-c) is no more than ¼, induced velocity limit is respected up to 4 cells of smearing. The number obtained is not really constraining and one can take a characteristic time inducing a very small light “wind”. In the future, it is not impossible that the characteristic time could be related to the turbulence parameters (that is by force to the local turbulence time).

One can also interpret this VOF sharpening algorithm as a pseudo-condensation algorithm.

While extremely simple, this algorithm is not adapted to every flow configuration. In effect, being as it is, it is not conservative, it requires that all the long living light phase volumes are in contact with a boundary where a stagnation inlet is set. A conservative form of the algorithm is foreseen in the near future as part of the work to perform in the THINS project.

6 Thermal coupling

The spallation target loop needs obviously to be thermally coupled with the proton beam. While the beam reference Energy (2.5 GeV) and current intensity (2 mA) are fixed, the beam size has been subject to variations.

The reference beam footprint size was bi-Gaussian with σ_x= 5cm and σ_y= 1 cm and cut at a distance of three σ.

In a second iteration σ_y has been enlarged to 1.5 cm with an apparent cut at 2 σ_y.

The σ values should be considered as maximum values. For a free-surface channel target with the flow running in the x direction, σ_x do not significantly influence the temperature maximum therefore we still have considered a value of 5 cm for the footprint on an horizontal surface even if the beam is inclined 45 degrees from the vertical. With this footprint and beam inclination, we get the same local power density as for a vertical beam with σ_x about 3.5 cm.

For constant heat release in z, the height of heat released has been quite artificially set to 50 cm.

Once the simulations have been successfully run with the beam heat release independent of z, Etam Noah from the ESS target team has run a Fluka simulation on a LBE block to get a better description of the beam heat release. He has also derived best fits, one "heavy" with about 20 parameters, and a "light" one described hereafter.

The light fit has the form: f(x,y,z)=f(z)*f(x,y), where f(x,y) is bi-Gaussian footprint profile. The depth profile has been fit in the following way:

$f(z)=\alpha \exp(-z/\beta) (1-\exp(-\gamma - z/\delta)$ (considering the z-axis downward).

the parameters, set in USI for a 2mA beam are: α= 2E12*0.00131 W/m^3, β=0.156 m, γ=0.654 (adim) and δ=0.0663 m.

The transformation to have the 45 degrees angle are the following: (i) $\alpha \rightarrow \alpha \sqrt{2}$, (ii) $z \rightarrow z \sqrt{2}$ and (iii) $x \rightarrow x + z$.

However, with these parameters, the total heat release was about 1.6 MW while the original raw data in Fluka gave 2.3 MW. As the heat released seemed correct close to the free surface, we have retrieved artificially the correct heat release by multiplying β by 1.4, slowing down therefore the heat release damping with depth.

From the numerical point of view, it is very difficult to take dynamically into account the exact local position of the free-surface, therefore some approximation is done by considering only the surface reference level: above this level, the heat release value is prolonged by continuity.

In the fast case, the beam footprint was in a rather varying free-surface region. The beam has thus been shifted to a more quiescent zone (15 cm downstream) before switching to the fitted heat deposition profile.

The trace of the beam heat release on the symmetry axis is shown on Figure 12 for the constant depth profile and on Figure 13 for the fitted depth profile.

7 Results and discussion

The simulations have been run for a certain time, until a reasonably constant mass flow rate has been reached, before resetting for restart and lighting the beam. Information related to the volume flow rate, the average velocity in the spallation zone and loop hydraulic resistance (equal to the pump thrust) at the final stage of the simulations are given in Table 2. Information regarding the

beam shape and size, the beam heat release, the maximum temperature on the free surface and in the LBE bulk are given in Table 3. We recall that the incoming LBE arrives in the spallation zone at 300 C.

The slow case has been run first with the reduced footprint for 5 s, results are illustrated on Figure 14. In this and following figure, the LBE flows counter-clockwise in the left picture and clockwise in the right picture (the plot has been obtained rotating the geometry by 180 degrees). Then the beam footprint has been enlarged and the simulation has been continued for another 5s (shown on Figure 15). Finally, the vertical profile has been installed and the simulation run for 5 s, with the results illustrated in Figure 16.

The fast case has been run first with the reduced footprint for 5 s, results are illustrated on Figure 17. By the time the simulation ended, the fitted beam profile was available, so the second foreseen case has been cancelled. The simulation has been directly pursued with the fitted beam for 5s but only 4s were available to trouble shooting with the java environment. At this time, the better adequacy of the slow case results to the ESS needs was clear and this last simulation was left as is.

Case	Volume flow rate	Velocity in the Spallation zone	Pump thrust
slow	14.1 l/s (28.2 l/s)	~ 0.6 m/s	5.2 kPa
fast	19.5 l/s (39.0 l/s)	~0.8 m/s	7.5 kPa

Table 2: Volume flow rate, typical velocity and pump thrust for the slow and fast cases.

Beam profile	$\sigma_{y.}$=1 cm constant in z	$\sigma_{y.}$=1.5 cm constant in z	σ_{y}=1.5cm. variable in z
Total Released Thermal Power, simulated domain, physical domain.	1.17 MW, 2.35 MW	2.33 MW, 4.67 MW	1.15 MW, 2.3 MW
Peak Thermal Power	1.5 kW/cm^3	2 kW/cm^3	2.23 kW/cm^3
Peak surface Power	1.5 kW/cm^3	2kW/cm^3	Slow:1.78 kW/cm^3, fast: 2.19 kW/cm^3
Slow case Max surface T	407 C	491 C	489 C
Slow case Max bulk T	439 C	524 C	510 C
Fast case Max surface T	404 C	Non simulated	451 C
Fast case Max bulk T	403 C	Non simulated	451 C

Table 3: thermal characteristics of the different simulations with 300 C incoming flows.

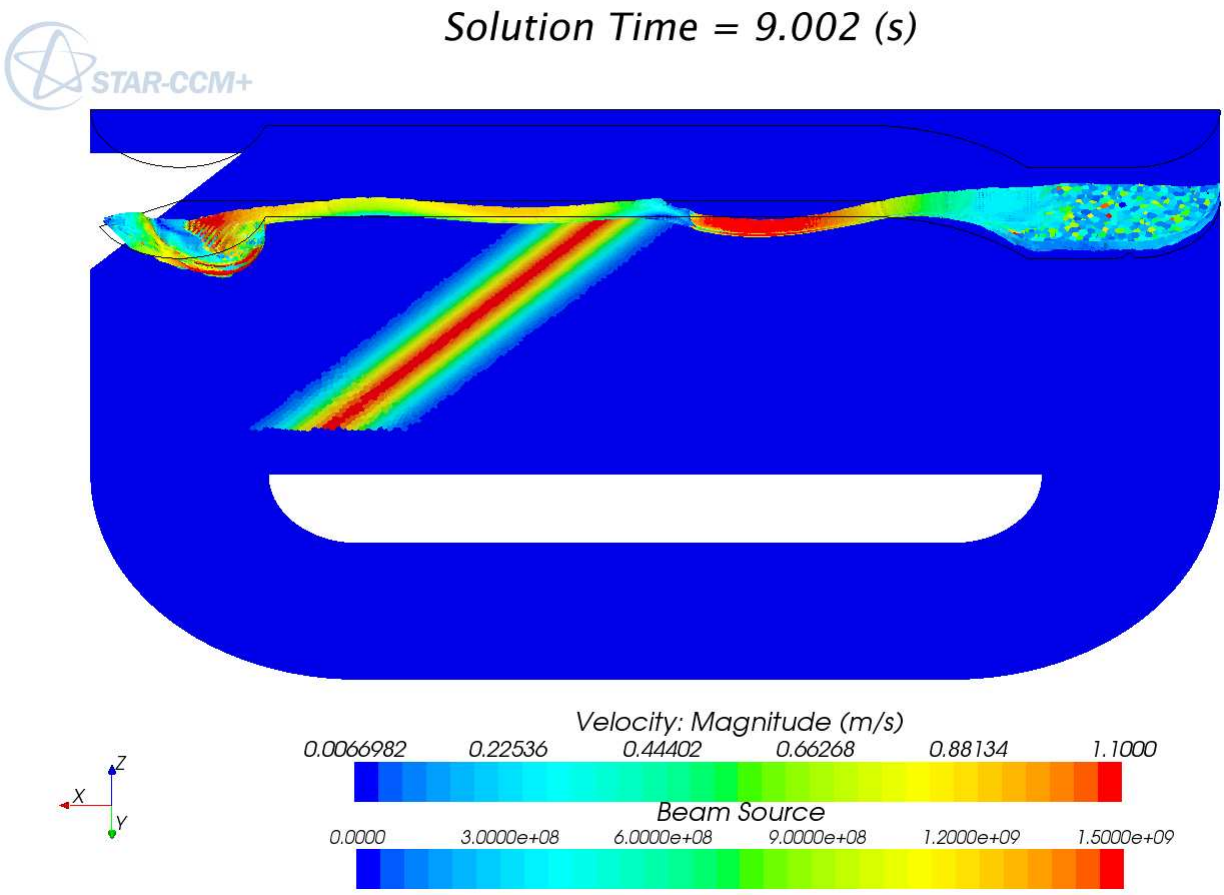

Figure 12: beam trace on the symmetry axis and velocity magnitude on the free-surface, fast case, fow counter-clockwise.

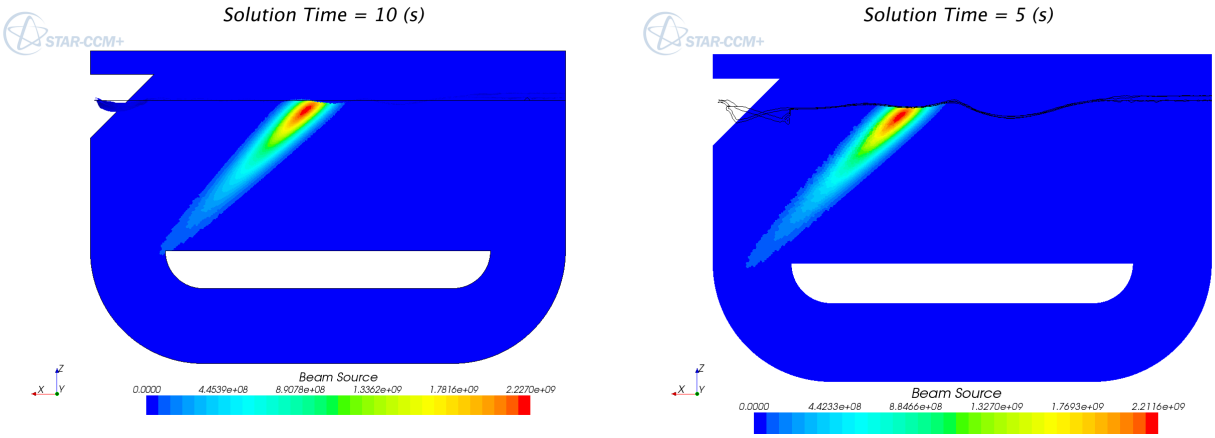

Figure 13: Beam source profile on the symmetry axis. Left: slow case, right: fast case.

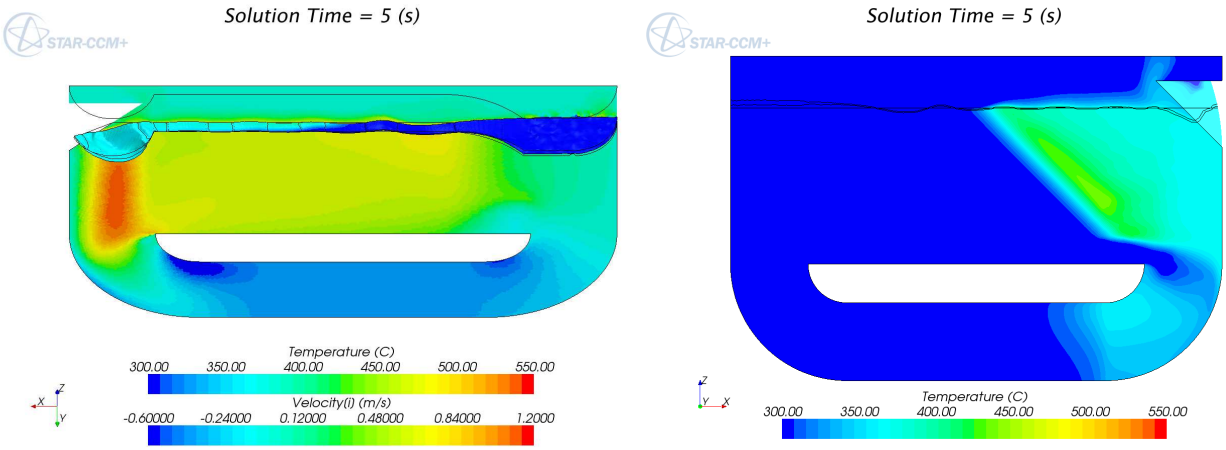

Figure 14: slow case with small footprint heat deposition ; temperature, free surface position and velocity field.

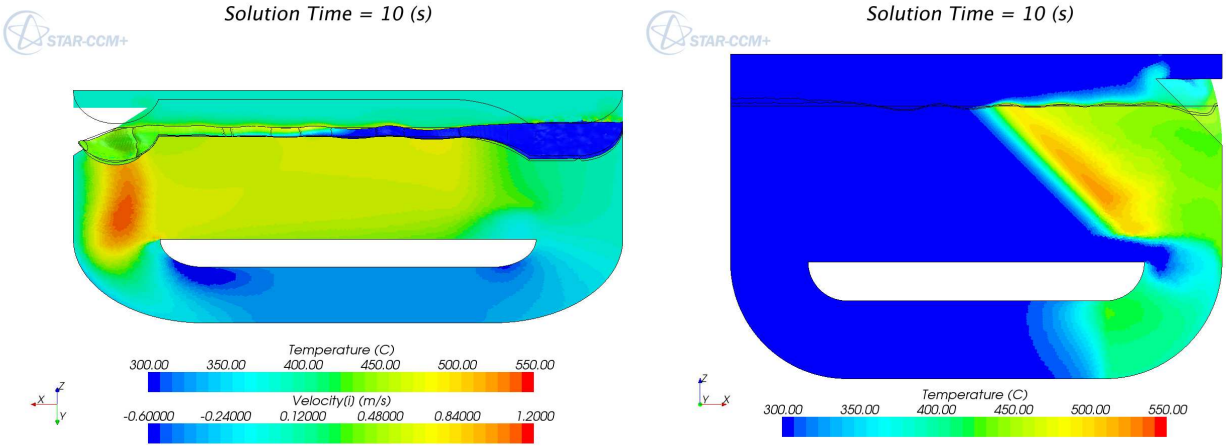

Figure 15: slow case with large footprint heat deposition ; temperature, free surface position and velocity field.

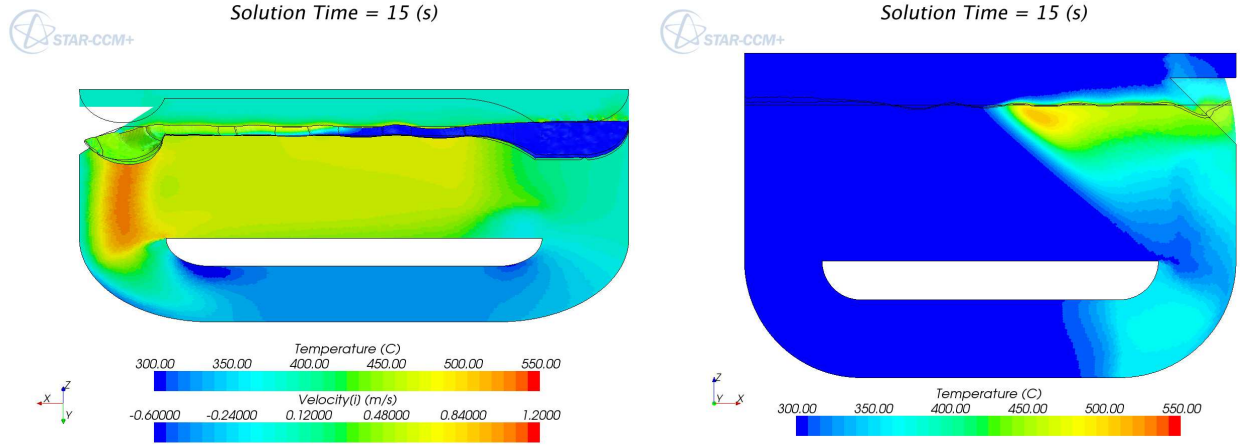

Figure 16: slow case with fitted heat deposition ; temperature, free surface position and velocity field.

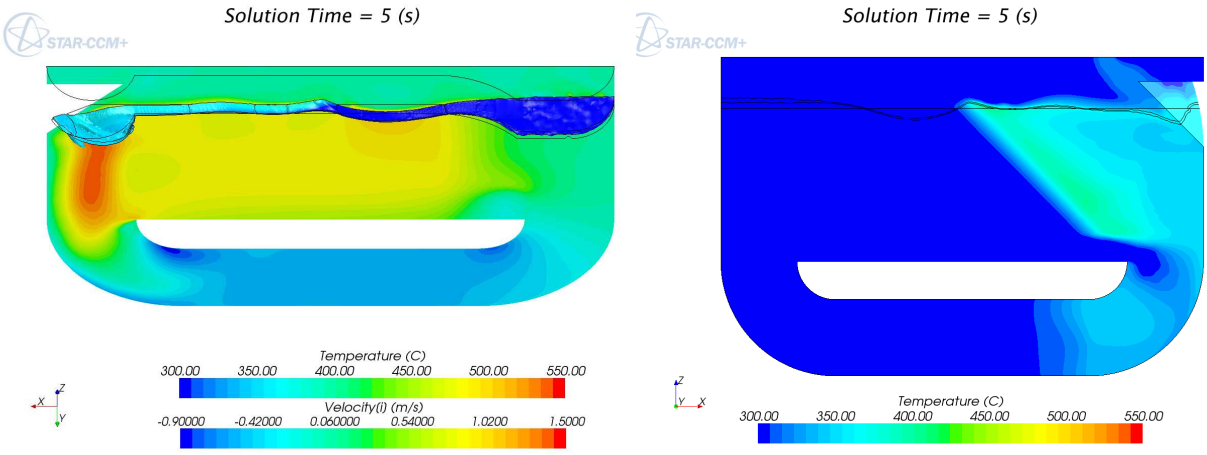

Figure 17: fast case with small footprint heat deposition ; temperature, free surface position and velocity field.

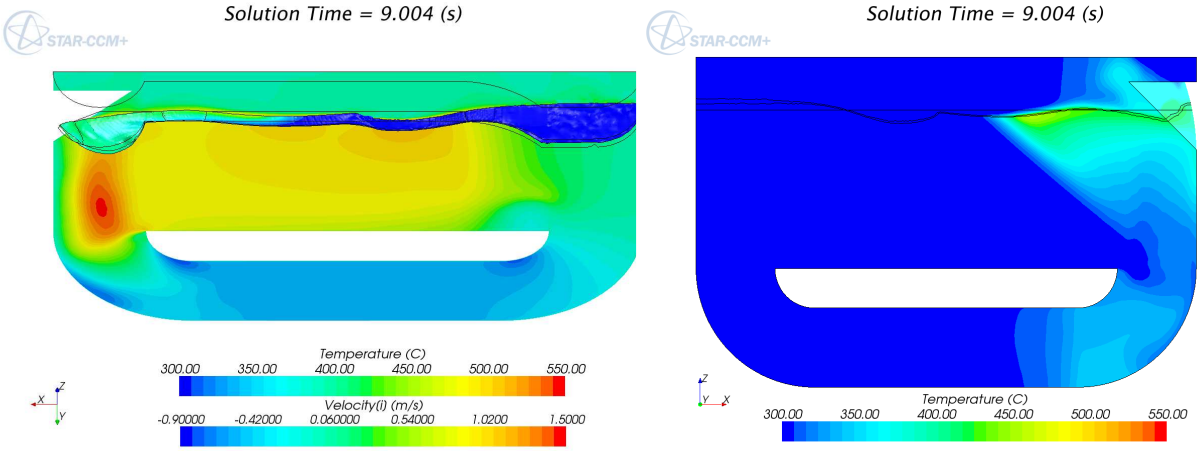

Figure 18: fast case with fitted heat deposition ; temperature, free surface position and velocity field.

From the hydraulic point of view, the two cases are quite different. Unfortunately, this difference can be fully appreciated only on the animations. In effect the slow case is almost stationary, even if the free-surface is not completely horizontal, while the fast case shows large oscillations of the free-surface with a time scale of order one or two seconds. From one hand, the fast case gives a good demonstration that the surface sharpening algorithm performs very well, being able to make the surface flow recover from surface wave breaking, nevertheless still giving the feeling that the surface is not artificially hardened. From the other hand, it is much more convenient for the ESS purpose to have a quasi stationary free-surface. Therefore, for the ESS application, that is, for thermal consideration, only the slow case will be analysed. Continuing on the hydraulic analysis, we should underline two extremely satisfying flow features:

- In both cases, the pressure losses associated with the spallation target region are extremely low, below 0.1 Bar.
- In contrast with the second Hg loop, no backward wave disturbs the flow. The ship prow-like obstacle performs very well its duty.

While the fast case experiments some occasional local backward flow, due to the wave breaking, in the slow case, the flow velocity is kept quite constant in the spallation region. Therefore, no unexpected hot point appears.

Most important is that the surface temperature is always kept below 500 C. This corresponds to a vapour pressure quite below 0.01 Pa as required. Moreover, the simulation is still meaningful with a temperature up to 150 K less with LBE, giving a very large margin for operative condition. On another hand, rising the temperature by 50 K, the loop can be operated with pure lead. In this case, the operative condition has less margin (before flow optimisation) but the maximum local vapour pressure is kept about 0.01 Pa.

It seems that 0.1 Pa is acceptable in the final part of the FASTEF beam line **[10**]. It is therefore probable that it will be also acceptable for the ESS beam line. By keeping the vapour pressure below 0.01 Pa, we have margin for the evaporation of the spallation products. These spallation products would very conveniently be pumped out somewhere in the vacuum plenum above the free-surface. In this way, the vacuum plenum can be in direct contact with the beam line terminal part.

While apparently perfectly functioning, this design may be largely optimised. But before optimisation, the design will have to be slightly modified to cope with the real proton beam heat deposition. And as the proton beam heat deposition depends on the spallation target geometry, an iterative process must be undertaken.

The interaction of the protons with the spallation target deviates the protons from a perfectly straight trajectory. The result is that the heat is released in a more extended volume than the mere extrusion of the beam footprint. While this effect is negligible close to the free-surface, it becomes more and more relevant while going more and more in depth. This phenomena is very tricky because the heat released in the diffuse deep out-centred region has a density several orders less than the maximum heat release density. But if this heat is released in a stagnant, or worse, a solid region, for example a containment wall, it must be evacuated by conduction. And conduction is generally less efficient than convection by several orders. Both phenomena may compete and the result may be the occurrence of extremely hot spots far away from the maximum heat release. However, once the phenomena is understood, it is relatively easy to avoid it, as has already been done in **[11**]. With regard to our design, it will surely be necessary to enlarge a few centimetres the bottom part of the spallation region. As the neutron moderators, which must be as close as possible to the neutron source, are to be located in the upper part of the spallation region, there is no harmful effect in enlarging the lower part. The flow will have to be however adapted to keep the same surface velocity. It can be done either by slightly increasing the overall flow rate, or by profiling the flow. This is matter for further fine tuning optimisation.

There are several advantages in using such a spallation target. First of all, it is very simple. Only one fluid is operated in the sensible region. There is no critical structural part. The structures are subject to very low pressure loads (1 Bar or less). Operating under vacuum is extremely positive for the safety concern, because eventual leakages will cause gases to enter the highly contaminated region and not to leave it. In such cases, gas leakages are easy to detect because of the relative high pressure increase in the “vacuum”.

There is however a large “Damocles sword” pending on this design. The pulsed beam may cause the LBE to heavily cavitate and splash due to the pressure wave thermally induced by every beam pulse. This “Damocles sword” is common to all spallation target design and is surely much more critical for closed structure with necessarily a solid window, because of cycling stress fatigue. For the windowless channel target only peripheral not sensible structural parts are subject to this cycling stress. The liquid LBE rapidly recovers from it. However, a large amount of splashing could cause changes in the flow pattern, leading to a recirculation in the spallation region and consequently to an excessive temperature. Moreover, relatively large variations in the free-surface level would lower the efficiency of the neutron moderators.

The occurrence of cavitation induced splashing is extremely difficult to quantify. The problem is to evaluate how much traction for how much time a fluid is able to sustain without loosing its integrity. In theory, pure fluids should withstand easily an extremely high traction for a long time. In practice, due to solid and mainly gaseous impurities, fluids (water) begin to cavitate below the vapour pressure. The problem is that water always contains a large amount of extremely small bubbles which serve as seed for the disruption of the flow. For Mercury, a splashing experiment under the effect of a beam pulse has been qualitatively reproduced by setting a pressure threshold or -1.5 Bar for the destruction of the bond between SPH particles **[12**]. But the experiment was not performed with highly purified Hg under near vacuum. Operating with LBE under near vacuum, we can expect that the fluid will be cleared of almost all dissolved gaseous impurities and will contain almost no bubbles whatsoever. In this configuration, it is perfectly expectable that the LBE will be able to withstand much better than Hg the pressure disruption forces.

As preliminary simulations with the very conservative Hg parameter indicates possible small splashing up to few centimetres high, we can expect no splashing in reality. At least it would be worth the pain to dedicate an experiment to control the integrity of LBE under vacuum and under a beam effect. However, the small intensity of splashing predicted with the Hg parameter indicates that almost no splashing would occur with a slightly enlarged beam or with a slightly increased beam pulse duration, remembering than in a recent past, the ESS pulse was set to 2 ms and not 1 ms as it is now.

8 Conclusion

A series of CFD simulations has been performed in order to define a valid proposal for the ESS spallation target. A full 3D channel spallation loop with an articulated free surface and a thermal coupling has been investigated numerically with starccm+V5.02. This has been possible thanks to the use of a simple but apparently original condensation/sharpening algorithm. The sharpening algorithm performs very well, allowing to keep the interface almost everywhere and almost always no more than 2 cells wide. However, the surface still do not suffer from an artificial increased rigidity. The possibility to numerically investigate such articulated flow has allowed us to define a very promising design which could serve as a basis for the ESS spallation target..

9 Acknowlegment

The presented word has been financially supported partially by the Autonomous Region of Sardinia and partially by the European Commission (FP7 Euratom). Many thanks for the neutronic calculation and the useful discussion to the ESS Target Station team.

10 References

[1] ESS http://en.wikipedia.org/wiki/European_Spallation_Source

[2] Carluec, B., jardi, X., 2003. European project PDS XADS-preliminary design studies of an experimental accelerator driven system. In: Proc. Of the Int. Workshop on P&T and ADS Development, SCK-CEN,Mol,Belgium,p. A91

[3] J.U. Knebel et al. European Research Programme for the Transmutation of HighLevel Nuclear Waste in an Accelerator Driven System (EUROTRANS), Proc. 9th Int. Exchange Meetng on Partitioning & transmutation, Nimes France, September 25-29 2006.

[4] http://www.cd-adapco.com/.

[5] Moreau, V., Free Fall 2D+ Simulation with StarccmV4. Calculation report 10/55. CRS4, jul 2010. http://www.crs4.it/Publications/cgi-bin/tr/repository/crs4_1534.1.doc

[6] Moreau V.. Feasibility Study of a CRS4 Alternative Spallation Target for FASTEF. Calculation report 10/56. CRS4, jul 2010. http://www.crs4.it/Publications/cgi-bin/tr/repository/crs4_1535.3.doc

[7] Beaten P. et al., the Central Design Team FP7 projet, http://www-pub.iaea.org/MTCD/publications/PDF/P1433_CD/datasets/presentations/SM-ADS-09.pdf

[8] Handbook on Lead-bismuth Eutectic Alloy and Lead Properties, Material Compatibility, Thermal-hydraulics and Technologies, 2007 Edition,OECD/NEA Nuclear Science Committee, OECD 2007, NEA No.6195

[9] Cheng, X., THINS, http://www.ifrt.kit.edu/english/21_97.php

[10] L. Mansani, Ansaldo Nucleare. (Minutes of the) CDT WP2 2nd Technical Meeting, Mol 23-24 June 2010.

[11]Bianchi, F., et al, Thermo-hydraulic analysis of the windowless target system, Nucl. Eng. Des. (2008), doi: 10.1016/j.nucengdes.2007.10.026

[12] Massidda L., Kadi Y., SPH simulation of liquid metal target dynamics, Nucl. Eng. Des. (2010)